Rare Metal Materials and Engineering
Volume 52, Issue 1, January 2023
Available online at www.rmme.ac.cn

Science Press

Cite this article as: Wei Yulin, Shi Guopu, Chen Sique, et al. P-modified γ-Al_2O_3/α-Al_2O_3 Foams with High Porosity as Palladium-Catalyzed Carriers[J]. Rare Metal Materials and Engineering, 2023, 52(01): 87-94.

ARTICLE

P-modified γ-Al_2O_3/α-Al_2O_3 Foams with High Porosity as Palladium-Catalyzed Carriers

Wei Yulin[1], Shi Guopu[1], Chen Sique[1], Yang Hailing[1], Ji Jun[1], Chen Yingying[1], Li Xinyu[1], Ma Deli[1], Pan Baocai[1], Zhang Zhenyu[1], Wang Honglei[2]

[1] School of Materials Science and Engineering, University of Jinan, Jinan 250022, China; [2] Anhui Dexinjia Biopharm Co., Ltd, Fuyang 236600, China

Abstract: A novel method for the preparation of α-alumina foams with P-γ-Al_2O_3 modified coating for the palladium catalysts was proposed. The polyurethane template method was used and the preparation parameters were optimized. The apparent porosity of the ceramic foam is 90.28%, the bulk density is 0.45 g·cm^{-3}, and the strength of ceramic foam is satisfying. The P-modified γ-Al_2O_3 coating was prepared on the α-alumina foam, and then the active catalytic phase (Pd) was loaded by ultrasound-assisted impregnation. Results show that the P-containing coating increases the surface area and weakly acidic sites of the inert foam while decreasing the proportion of strongly acidic sites. Compared with the uncoated foam, the foam with modified coating can easily load the active phase. In addition, the loaded Pd metal can hardly be oxidized, and the catalytic conversion temperature (T_{50}, T_{90}) of CO reduces by about 50 °C. This research presents the great practical potential of low-cost modified α-Al_2O_3 ceramic foams in the palladium catalyst production.

Key words: γ-Al_2O_3/α-Al_2O_3 foams; palladium catalyst; P-modification; high porosity; CO catalytic combustion

Pd catalysts with unfilled *d*-electron orbitals have the advantages of ligand diversity and good capacity to absorb/detach groups, therefore being essential in catalytic engineering, waste gas treatment[1], petrochemicals[2], and drug production[3]. The multiphase catalysts with palladium loaded on solids have been widely researched, because they can solve the drawbacks of large usage, high residue, and low utilization ratio of homogeneous catalysts. Alumina[4-6] is one of the most promising solid-phase carriers for the multiphase catalysis. Porous γ-Al_2O_3 with enormous internal surface area, high activity, and strong adsorption capacity is often used as the catalytic carrier. α-Al_2O_3 has the advantages of high strength, excellent corrosion resistance, fine thermal stability, and low cost.

Doping metallic elements, such as Ba, Ce, and Mg[7–10] is a common method to enhance the catalytic performance. Some methods use the non-metallic (B, P, Si)[11–13] or noble metal components. Chen et al[14] found that the Pd/P-Al_2O_3 catalysts affect the catalytic performance for the conversion of hydrocarbon, CO, and NO_x due to the enhanced adsorption property and reducibility of P-modified mesoporous Al_2O_3.

Normally, the catalytic carriers are granular[15]. However, the foam ceramic is a monolithic carrier with short internal diffusion path, high mass transfer efficiency, and superb hydrodynamic properties, which is better than the conventional catalytic carrier of Rasching ring structure. The foam ceramics can be prepared by the pore formation agent, template, foaming agent, lyophilization, and sol-gel methods[16–19]. Among them, the template method[20] is a simple process with low cost, and the microstructure and morphology of the formed material can be adjusted by changing the organic foam. Although α-Al_2O_3 can be used to manufacture foam ceramics, it is rarely used as catalytic carrier due to its small specific surface area (typically, the surface area of α-Al_2O_3 is $1-5$ m^2·g^{-1})[21–22]. Only a few surface acidic sites exist in α-Al_2O_3, and it is too stable to be modified. Furthermore, the apparent porosity of α-Al_2O_3 foams is low[23]. Therefore, the lightweight catalytic carriers with high porosity

Received date: March 26, 2022
Foundation item: National Natural Science Foundation of China (51872118, 51632003); Shandong Province Key Research and Development Plan (2020JMRH0401, 2019RKB01018); Shandong Provincial Natural Science Foundation (ZR2018PEM008, ZR2019MEM055)
Corresponding author: Shi Guopu, Ph. D., Associate Professor, School of Materials Science and Engineering, University of Jinan, Jinan 250022, P. R. China, Tel: 0086-531-89736986, E-mail: ss_shigp@ujn.edu.cn

are required.

In this research, α-Al_2O_3 foams modified by γ-Al_2O_3 coating doped with P element were prepared and used for Pd catalysts. The preparation of α-Al_2O_3 foam ceramics involves the polyurethane template and the impregnation-blowing-drying-sintering process. Thus, the influence of process parameters on the foam properties was investigated. The foam carriers were modified by P-doped γ-Al_2O_3 coating, and the Pd catalysts were prepared by the ultrasound-assisted impregnation and roasting-reduction procedures. The catalytic combustion activity at low CO content was evaluated, and the modification mechanism of the coatings was discussed. This research presented the great practical potential of low-cost modified α-Al_2O_3 ceramic foams in the palladium catalyst production.

1 Experiment

The ratio of raw material slurry used in this research is shown in Table 1. To obtain the homogeneous slurry, the mixed slurry was poured into the resin ball mill tank and milled for 6 h. The polyurethane foams with pore densities of 20 PPI, 25 PPI, and 30 PPI (PPI stands for the pores per linear inch) were used and named as 1#, 2#, and 3# templates, respectively. The templates were washed by water and ethanol and then immersed in NaOH solution (10wt%–20wt%) for 12 h. Afterwards, the templates were cleaned, dried, and immersed in 5wt% polyvinyl alcohol (PVA) solution for 12 h. These pretreated polyurethanes were impregnated in the slurry and blown by warm airflow to remove the leftover slurry which clogged the through-hole. The dried specimens were placed in a sintering furnace at high temperatures, and the heating procedure is shown in Fig. 1. Different heating rates were used when the heating temperature rose from 200 °C to 500 °C.

The coating slurry was γ-Al_2O_3 and γ-Al_2O_3 doped with 3wt% phosphoric acid. The coating specimens were immersed in the slurry and blown to remove the excess slurry. The coating specimens were calcined at 600 °C for 6 h. The uncoated foam, the foam with γ-Al_2O_3 coating, and the foam with P-modified γ-Al_2O_3 coating were named α-A, γ/α-A, and P(γ/α-A), respectively. Before the catalyst preparation, the contaminants in the carrier pores must be eliminated by high temperature treatment for a long time.

The active Pd substance of 8wt% was loaded on the foam by impregnation method. The palladium nitrate solution was diluted by ammonia with the equal volume. Then the foam carriers were immersed in the diluted palladium nitrate solution and placed in an ultrasonic dispersion apparatus for 1 h. Afterwards, the foam carriers with Pd solution were heated by water bath for 1 h and left to stand for 12 h. Finally, the foam was taken out of the solution and dried in an oven for 2 h. The dried specimens were then roasted at 350 °C for 2 h in a muffle furnace. The catalyst was reduced by 2wt% hydrazine hydrate solution for 12 h and then washed by deionized water before use. The catalysts formed by α-A, γ/α-A, and P(γ/α-A) foams were named as Pd-(α-A), Pd-(γ/α-A), and Pd-P(γ/α-A), respectively.

The thermal stability and volatilization temperature of polyurethane templates were examined by the NETZSCH STA-449F3 thermogravimetric analysis instrument. The apparent porosity of post-fired ceramic foams was examined by the Archimedes method according to GB/T 2997-2005 standard, and the bulk density of the ceramic foams was determined according to GB/T 2999-2016 standard. The post-fired length of the specimens was measured by MNT-150T vernier caliper (Shanghai Menet Industrial Co., Ltd), and the post-fired linear shrinkage of porous foam ceramics was calculated according to GB/T 5988-2007 standard. The compressive strength of the specimens was determined by CMT5105 electronic universal testing machine (Shenzhen New Sansi Materials Testing Co., Ltd). Thermo Fisher Scientific MARS40 rheometer was used to study the rheological properties of slurry. The foam morphology was observed by scanning electron microscope (SEM, Quanta 250

Table 1 Ratio of raw material slurry

Specimen	Raw material/g						Solid content/wt%
	Al_2O_3	PVA	Carboxymethyl cellulose (CMC)	Nonionic polyacrylamide (NPAM)	Polyacrylic amide (PAM)	H_2O	
A1	19	0.3	-	0.2	0.5	80	20
B1	19	-	0.3	0.2	0.5	80	20
A2	24	0.3	-	0.2	0.5	75	25
B2	24	-	0.3	0.2	0.5	75	25
A3	29	0.3	-	0.2	0.5	70	30
B3	29	-	0.3	0.2	0.5	70	30
A4	34	0.3	-	0.2	0.5	65	35
B4	34	-	0.3	0.2	0.5	65	35
A5	39	0.3	-	0.2	0.5	60	40
B5	39	-	0.3	0.2	0.5	60	40
A6	44	0.3	-	0.2	0.5	55	45
B6	44	-	0.3	0.2	0.5	55	45

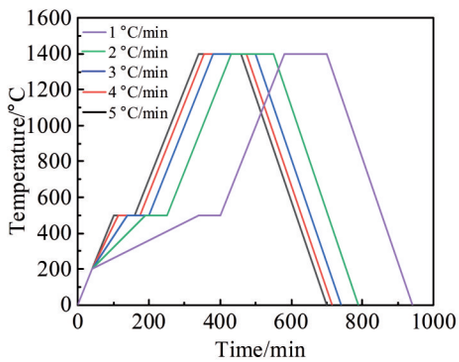

Fig.1 Heating procedures for foam preparation with different heating rates at 200–500 °C

FEG, FEI, USA).

The X'Pert PRO MPD X-ray diffractometer (XRD) was used to analyze the phase composition of the foam carriers and catalysts. X-ray photoelectron spectroscope (XPS) with Thermo Scientific K-Alpha equipment was used to determine the valence of the catalytic active Pd component. The specific surface area (BET) of foams and catalysts was calculated by the Quantachrome 4000E equipment and porosity analyzer. The AutoChem1 II Model 2920 programmed temperature rise chemisorption analyzer (TPD) was used to analyze the surface properties of the specimens. The catalyst morphology was also studied by SEM. The EDAX TEAMEDS energy dispersive spectrometer (EDS) was used to investigate the element distribution on the catalyst surface.

In the quartz tube type atmospheric pressure flow-through fixed bed reactor, the oxidation of CO with low content was conducted as a model reaction. The ratio of feeding gas was $CO:O_2:N_2=1:10:89$, and the total gas flow rate was 50 $mL\cdot min^{-1}$. CO and O_2 were reaction gases, N_2 was equilibrium and purge gas, and the catalyst dosage was 50 mg. The reaction temperature was controlled by a thermocouple in the quartz tube at the center of catalyst bed, and the temperature was increased at heating rate of 2 $°C\cdot min^{-1}$ after the detector was stabilized. An Angilent-6850 gas chromatograph was used to evaluate the reactants and products, and the catalytic activity of catalyst was determined by CO conversion.

2 Results and Discussion

2.1 Synthesis and properties of foams

2.1.1 Thermal properties of template and linear shrinkage of foam

The bulk density, apparent porosity, mechanical strength, and carrier quality can be improved by optimizing the process parameters, thus reflecting the influence of process parameters on the properties of foam ceramics. The template is crucial. The foam surface was processed by strong alkali NaOH solution and PVA to eliminate the surface interlayer and increase the surface roughness, because the smooth and hydrophobic surface cannot be uniformly covered by water-based ceramic slurry. The thermogravimetric (TG) curves and differential scanning calorimetric (DSC) curves of polyurethane foam are shown in Fig.2. The polyurethane foam decomposes rapidly and loses mass since 200 °C. The mass loss rate increases after 340 °C because the polyol in the residual foam begins to decompose and releases gas until 400 °C. The mass of the final residual foam is only 6.77% of that of original foam. The water vaporization of the polyurethane foam results in the heat absorption peak at 100 °C, and the other two heat absorption peaks are due to the decomposition of organic substances or functional groups, which corresponds to the inflection points in DSC curve. As a result, the polyurethane foam primarily decomposes and volatilizes at 200–500 °C. If the temperature rises too fast in this process, the organic substance will be violently oxidized and swiftly release a large amount of gas to impact the blank, causing violent shrinkage and even cracking and chalking, and damaging the quality and performance of porous ceramic foams.

Table 2 shows the linear shrinkage of ceramic foams after heating at 200 – 500 ° C. Fast heating rate may cause the reduction in specimen size and even specimen collapse. According to Fig. 3a, the ceramic pillar is hollow inside and the spherical expansion bubbles are generated on the surface due to the impact of gas generated by the decomposition of polyurethane. If the impact is strong, a local blowout and an open hole can be generated. Besides, the faster the heating rate, the intenser the gas release and the more the generated pores. The pillar shrinks when the small pores are densified, i.e., the more the densified pores, the more obvious the foam shrinkage.

2.1.2 Foam morphology

Fig.3 shows SEM morphologies of the ceramic foams. The

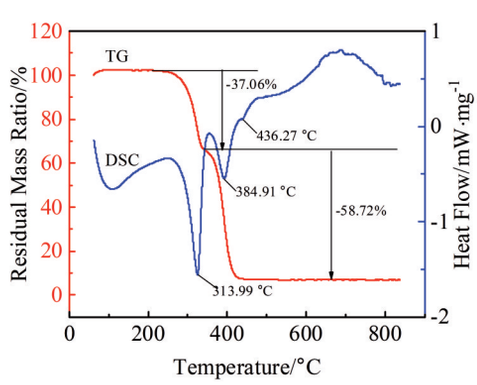

Fig.2 TG and DSC curves of polyurethane foam template

Table 2 Linear shrinkage of ceramic foam

Heating rate/°C·min^{-1}	Linear shrinkage/%			Specimen integrity
	Height	Length	Width	
1	8.7	12.5	11.8	Complete
2	11.4	12.7	13.6	Complete
3	13.5	16.3	16.8	Complete
4	17.6	20.4	22.3	Defected
5		-		Collapse

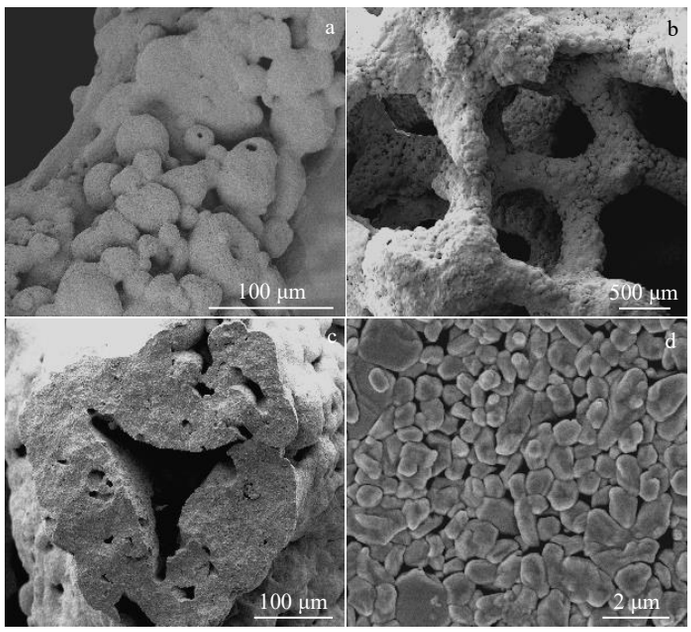

Fig.3 SEM morphologies of ceramic pillar surface (a), mesh structure (b), cross-sectional triangular pores (c), and grains (d) in α-Al_2O_3 ceramic foams

ceramic pillars consist of uniform coarse pores with size larger than 500 μm. The polyurethane firing causes typical hollow triangular pores at the joints, and the pore diameter is larger than 100 μm. The swollen foam-like spherical protrusions exist on the pillar surface, which consist of small open pores of 1–10 μm in size. This shape can increase the surface area and the amount of active alumina coating on the foam. It can be observed that the ceramic particles are not dense and are distributed with pores of less than 1 μm. These pores originate from the filling of pores in the interstices of the alumina particles by additives.

2.1.3 Binder, solid content, and template pore density

The preparation procedure and performance of ceramic foams are also influenced by the slurry and template. Fig. 4a shows the porosity and bulk density curves of 2# template. It can be seen that when the solid content is 20wt% , the

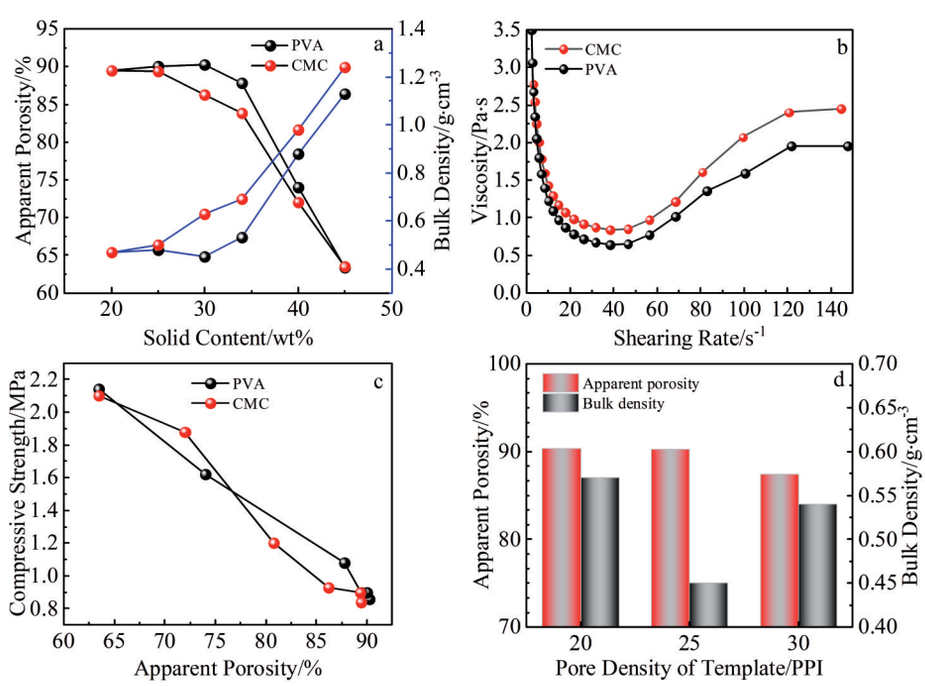

Fig.4 Apparent porosity and bulk density of ceramic foams (a) and templates (d); rheological properties of slurries (b); compressive strength of ceramic foams (c)

difference in porosity and bulk density is small with PVA as binder or CMC as binder. When the solid content increases to 30wt%, the difference is the most obvious: the maximum porosity is 90.28% and the bulk density is 0.45 $g \cdot cm^{-1}$ for the A3 specimen (PVA as binder). With further increasing the solid content, the difference is reduced gradually: the apparent porosity decreases and the bulk density increases. In addition, the apparent porosity of the foam specimens with PVA as binder is always higher than that with CMC as binder.

CMC molecular chains have strong intermolecular forces, which can form a solid grid structure. The alumina particles enter into the grid and are tightly bonded, thus reducing the zeta potential and presenting good bonding performance. Similarly, PVA is a water-soluble polymer made of polyvinyl acetate alcohol, and the hydrolysis produces a large number of hydrophilic hydroxyl groups, thus forming a stable macromolecular network structure between the molecules, which can be adsorbed on the particle surface and promote the particle slip, adhesion, and plasticity. CMC and PVA have similar rheological properties, which present the shear-thinning effect at low shear rates and shear-thickening effect at high shear rates, as shown in Fig. 4b. However, the slurry containing CMC binder has greater bonding strength than that containing PVA binder. The impregnation-blowing procedure demands a slurry with slow viscosity to prevent the clogged through-holes. When the solid content is low, the amount of residual slurry increases for stable specimen formation. Thus, the influence of the binder is slight, resulting in neglectable difference in apparent porosity and bulk density. With increasing the solid content, the amount of residual slurry is decreased and the influence of binder is more obvious. When the solid content is too high, which exceeds the maximum number of particles bonded by CMC mesh, the bonding strength is reduced. According to Fig. 4c, the compressive strength of specimens with PVA/CMC binder is decreased with increasing the apparent porosity. When the apparent porosity reaches 90.28%, the compressive strength is about 0.8 MPa, which satisfies the industry product requirement.

Fig. 4d shows the performance of ceramic foams prepared by templates of different pore densities. The ceramic foam prepared by 1# template (20 PPI) has the highest porosity. The 1# template has the smallest pore size of 1.27 mm and the thinnest 3D network structure, resulting in a thick slurry coating on the foam surface for the stable development, thereby increasing the workload. The ceramic foam prepared by 2# template (25 PPI) has a solid structure with high apparent porosity, which is only 0.03% lower than that prepared by 1# template, therefore exhibiting the optimal properties.

2.2 XRD and XPS analyses of foam catalysts

XRD patterns of the foam and catalysts are shown in Fig. 5. It can be seen that the foam and catalysts are mainly composed of corundum phase (α-Al_2O_3, PDF card number: 75-1865) and a minor amount of mullite phase ($Al_6O_{13}Si_2$, PDF card number: 89-2645). No diffraction peaks of Pd, P, or γ-Al_2O_3 can be observed, which can be attributed to their low content and the highly dispersed Pd particles. The impurities after sintering produce a minor amount of mullite, which improves the corrosion resistance and thermal stability of foam, thereby widening the application of ceramic foam catalysts. The crystal structure of α-Al_2O_3 is tripartite, its theoretical density is 3.99 $g \cdot cm^{-3}$, the melting point is 2050 °C, and the Mohs hardness is 9.

$PdNO_3$ combining with ammonia during the impregnation process can generate $[Pd(NH_4)_4](NO_3)_2$, which adheres to the alumina foam carrier and then is transformed to the stable palladium oxide by roasting. The alkaline impregnation solution reduces the acidic strength of carrier and increases the hydrothermal stability and activity of catalyst under certain conditions. Fig. 6 shows XPS spectra of foam catalyst

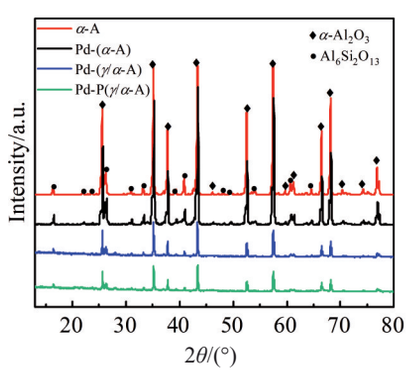

Fig.5 XRD patterns of foam and different foam catalysts

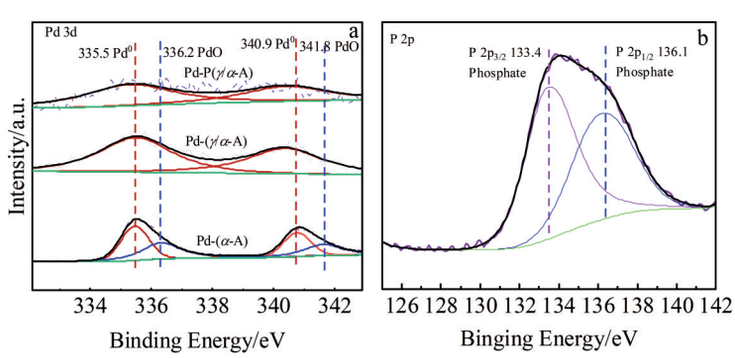

Fig.6 XPS spectra of Pd (a) and P (b) in foam catalyst

after reduction by hydrazine hydrate. The peaks of Pd $3d_{5/2}$ in Pd-(α-A) foam catalyst occur at 335.5 and 336.2 eV, which coincide with the results of 335.3 and 336.0 eV, respectively[8,23]. This phenomenon indicates that these two peaks originate from Pd^0 and PdO with the ratio of 6:4. This may be attributed to the non-in situ detection: some Pd metal is re-oxidized before detection, or some PdO is not reduced. The Pd^0 peaks in Pd-(γ/α-A) and Pd-P(γ/α-A) catalysts suggest that the coatings can prevent the oxidation of active metal phase. The addition of P element to the foam surface influences the reduced peak intensity in Pd-P(γ/α-A) catalyst. The peaks of P 2p occur at 133.4 and 136.1 eV, indicating the existence of the P element as phosphate. The P element can react with γ-Al_2O_3 to produce the P-O-Al phase and introduce vacancies.

2.3 Surface area and pore structure of foam catalysts

The surface areas of different foam catalysts were measured by the nitrogen adsorption method. The specific surface area BET and pore volume of these specimens are summarized in Table 3. The specific surface area and pore volume of Pd-(γ/α-A) catalyst are 20 and 129 times greater than those of the uncoated Pd-(α-A) catalyst, respectively. The rise in specific surface area is caused by the increase in γ-alumina content. The P-doping and active phase deposition reduce the specific surface area and pore volume. However, their effect is not significant. It is found that a modest quantity of coating can significantly increase the specific surface area of inert alumina foam.

Table 3 Specific surface area BET and pore volume of foam and catalysts

Specimen	Coating content/wt%	Foam content/wt%	BET/ $m^2 \cdot g^{-1}$	Pore volume/ $cm^3 \cdot g^{-1}$
α-A	0.00	100.00	1.3633	0.0020
Pd-(α-A)	0.00	100.00	0.8288	0.0010
Pd-(γ/α-A)	0.89	99.11	4.5918	0.0423
Pd-(γ/α-A)	2.34	97.66	17.8655	0.1293
Pd-P(γ/α-A)	2.22	97.78	13.1900	0.0856

2.4 SEM-EDS analyses of foam catalysts

SEM morphologies and corresponding EDS element distributions are shown in Fig. 7. It can be seen that the palladium particles are widely dispersed on the alumina surface and in the pores of alumina grains. The grain size of alumina in Fig.7b is much smaller, which can be attributed to the addition of γ-Al_2O_3 coating. The loading amount of palladium is larger in Pd-P(γ/α-A) catalyst, as shown in Fig. 7c. However, the Pd aggregation occurs. This is owing to the existence of highly concentrated Al-OH groups in γ-Al_2O_3 aggregates. This group can load more palladium than α-Al_2O_3.

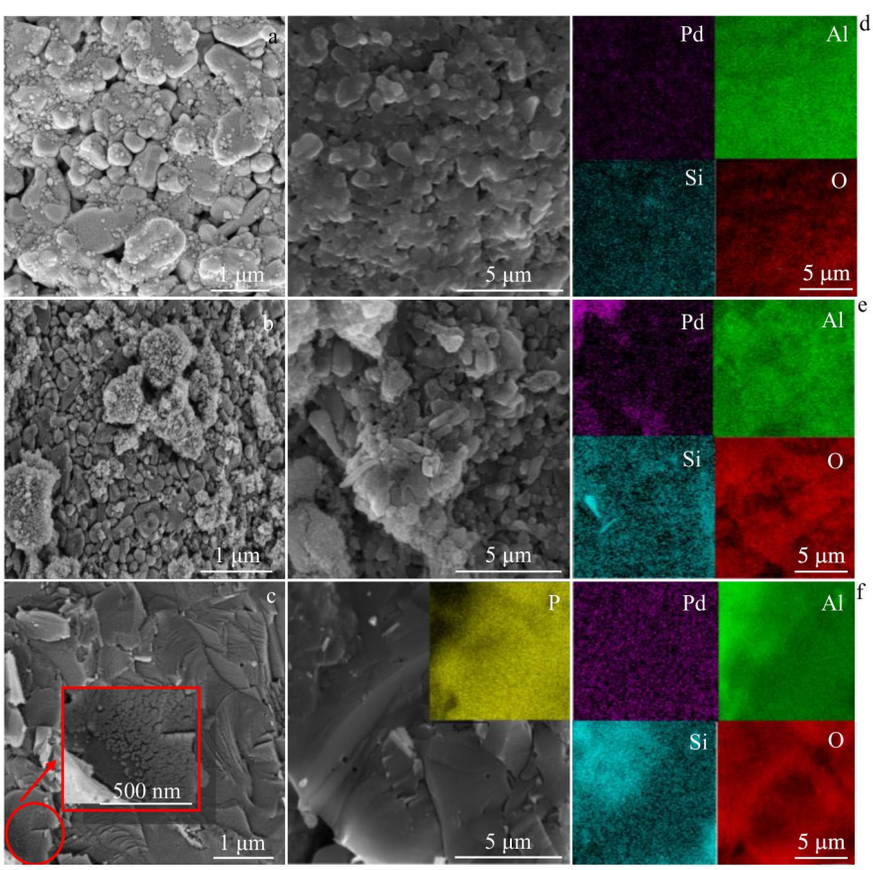

Fig.7 SEM morphologies (a–c) and corresponding EDS element distributions (d–f) of Pd-(α-A) (a, d), Pd-(γ/α-A) (b, e), and Pd-P(γ/α-A) (c, f) foam catalysts

A streak-like morphology appears on the grains, which is caused by the fine particle aggregation. This is because the reactive alumina and nanoscale P-O-Al phases are formed. In Fig.7f, the palladium is evenly distributed, and the Pd loading amount is obviously larger due to the P-doping in coating, which increases the defects and vacancies and improves the catalyst capacity to anchor the active phase. These results suggest that the modified γ/α-A and P(γ/α-A) foams can obtain a larger Pd loading amount.

2.5 Acidic sites of foam catalysts

The acidic properties of all foam catalysts were measured by NH_3-TPD method at 50–600 °C, as shown in Fig.8. It can be seen that the peaks at temperatures below 250 °C correspond to the weakly acidic sites, while those at temperatures above 250 °C correspond to the strongly acidic sites. There are two stages: one is the surface hydroxyl groups (-OH) serving as Bronsted acid sites by releasing a proton, and the other is the cationic metal centers acting as Lewis acid sites[24]. The surface of Pd-(α-A) catalyst has only a few strongly aci-dic sites provided by Pd element, while the Pd-(γ/α-A) and Pd-P(γ/α-A) catalysts contain more acidic sites due to the modified coating. The proportion of weakly acidic sites on the surface of Pd-(γ/α-A) catalyst is 34.6%, whereas that of Pd-P(γ/α-A) catalyst is 51.0%, indicating that adding P ele-ment can reduce the strongly acidic sites.

2.6 CO catalytic combustion

The direct combustion temperature of CO in industrial waste gas treatment and automotive exhaust treatment is 650–800 °C, while the catalytic combustion temperature is 250–400 °C. Generally, the complete oxidation temperature of CO is 300 °C. Huang et al[25] found that the initiation temperature of CO catalytic conversion with Pd/CeO_2-ZrO_2 catalyst is T_{50}= 239–334 °C.

Fig.9 shows the CO catalytic performance curves of different catalysts. For the Pd-(α-A), Pd-(γ/α-A), and Pd-P(γ/α-A) catalysts, the temperatures for 50% conversion (T_{50}) are 198, 210, and 247 °C, and the temperatures for 90% conversion (T_{90}) are 216, 219, and 270 °C, respectively. It is found that the catalytic temperature of catalyst with P-modified coating decreases by about 50 °C, compared with that of the Pd-(α-A) catalyst. The improved performance is due to the increased specific surface area, increased Bronsted acidic sites, and decreased strongly acidic sites.

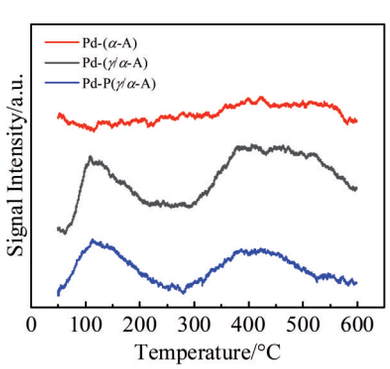

Fig.8 NH_3-TPD profiles of different foam catalysts

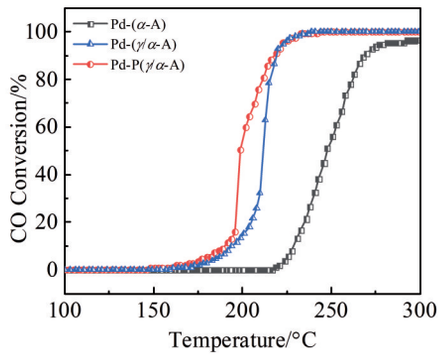

Fig.9 CO conversion by different foam catalysts

3 Conclusions

1) The polyurethane template with pore density of 25 PPI (PPI stands for the pores per linear inch) and PVA binder shows the optimal properties.

2) The temperature should be 200–500 °C at heating rate of 1 °C·min^{-1} during the foam sintering process to obtain the complete foam without defects. The finished foam has the apparent porosity of 90.28%, bulk density of 0.45 g·cm^{-3}, and compressive strength of over 0.8 MPa.

3) The P-modified alumina coating can enhance the adsorption of active phase of the ceramic foams, inhibit the Pd oxidation, increase the specific surface area and weakly acidic sites, and reduce the strongly acidic sites. In addition, the temperature for CO conversion reduces by more than 50 °C, compared with that without coating.

References

1 Miller J B, Malatpure M. *Applied Catalysis A: General*[J], 2015, 495: 54

2 Feng J T, Wang H Y, Evans D G *et al*. *Applied Catalysis A: General*[J], 2010, 382(2): 240

3 Gniewek A, Ziółkowski J J, Trzeciak A M *et al*. *Journal of Catalysis*[J], 2008, 254(1): 121

4 Rybakov A A, Bryukhanov I A, Larin A V *et al*. *Catalysis Today*[J], 2020, 357: 368

5 Chen Y, Wang N N, Ola O *et al*. *Materials Science and Engineering R: Reports*[J], 2021, 143: 100 589

6 Fedotov A S, Uvarov V I, Tsodikov M V *et al*. *Chemical Engineering and Processing-Process Intensification*[J], 2021, 160: 108 265

7 Li Na, You Hong, Yao Jie *et al*. *Journal of Harbin Institute of Technology*[J], 2007, 39(12): 1873 (in Chinese)

8 Huo Q H, Yue C X, Wang Y H *et al*. *Chemosphere*[J], 2020, 249: 126 164

9 Zhan Y Y, Kang L, Zhou Y C *et al*. *Journal of Fuel Chemistry and Technology*[J], 2019, 47(10): 1235

10 Zhao Ming, Wang Hairong, Cai Li *et al*. *Rare Metal Materials and Engineering*[J], 2010, 39(3): 519 (in Chinese)
11 Xiong Z Q, Mi Z T, Zhang X W. *Catalysis Communications*[J], 2007, 8(3): 571
12 Autthanit C, Khaochartchai C, Praserthdam P *et al*. *Catalysis Communications*[J], 2021, 148: 106 169
13 Labalme V, Beguin B, Gaillard F *et al*. *Applied Catalysis A: General*[J], 2000, 192(2): 307
14 Chen X H, Zheng X H, Lin W Z *et al*. *Powder Technology*[J], 2018, 338: 860
15 Buelna G, Lin Y S. *Microporous and Mesoporous Materials*[J], 1999, 30(2–3): 359
16 Rezaee S, Ranjbar K, Kiasat A R. *Ceramics International*[J], 2020, 46(1): 893
17 Luchini B, Storti E, Wetzig T *et al*. *Journal of the European Ceramic Society*[J], 2019, 39(8): 2760
18 Finhana I C, Machado V V S, Santos T *et al*. *Ceramics International*[J], 2021, 47(11): 15 237
19 Tang Y F, Mao M C, Qiu S *et al*. *Ceramics International*[J], 2018, 44(1): 1187
20 Shumilov V, Kirilin A, Tokarev A *et al*. *Catalysis Today*[J], 2022, 383: 64
21 Wang Hai, Liu Junjie, Song Xiaoping *et al*. *Chemical Analysis and Meterage*[J], 2014, 23(5): 1 (in Chinese)
22 Nor M A A M, Hong L C, Ahmad Z A *et al*. *Journal of Materials Processing Technology*[J], 2008, 207(1–3): 235
23 Huang W, Zuo Z J, Han P D *et al*. *Journal of Electron Spectroscopy and Related Phenomena*[J], 2009, 173(2–3): 88
24 Glazneva T S, Kotsarenko N S, Paukshtis E A. *Kinetics and Catalysis*[J], 2008, 49(6): 859
25 Huang Zhengwen, Guo Weiqi, Jiang Zhi *et al*. *Journal of Molecular Catalysis*[J], 2019, 33(1): 10 (in Chinese)

用于钯催化载体的P改性高孔隙率γ-Al_2O_3/α-Al_2O_3泡沫

魏郁林[1]，史国普[1]，陈嗣确[1]，杨海玲[1]，冀　珺[1]，陈莹莹[1]，李新宇[1]，马德礼[1]，潘保财[1]，张振宇[1]，王红磊[2]
(1. 济南大学 材料科学与工程学院，山东 济南 250022)
(2. 安徽德信佳生物医药有限公司，安徽 阜阳 236600)

摘　要：提出了一种新方法来制备用于钯催化剂的P-γ-Al_2O_3涂层改性的α-Al_2O_3泡沫。采用聚氨酯模板法，通过优化工艺参数，使陶瓷泡沫的显气孔率达到90.28%，体积密度达到0.45 g·cm^{-3}，且该泡沫具有可使用强度。将掺有P元素的γ-Al_2O_3涂层涂覆在α-Al_2O_3泡沫上，然后通过超声波辅助浸渍法来装载活性催化相（Pd）。结果表明，含P涂层增加了惰性泡沫的比表面积和弱酸性位点，同时减少了强酸性位点的占比。与无涂层的泡沫相比，改性的泡沫更容易装载活性相，且装载的金属Pd不容易被氧化，CO的催化转化温度（T_{50}，T_{90}）降低了50 ℃左右。该研究证明了低成本改性α-Al_2O_3陶瓷泡沫在钯催化剂生产中具有极大的应用潜力。

关键词：γ-Al_2O_3/α-Al_2O_3泡沫；钯催化剂；P改性；高孔隙率；CO催化燃烧

作者简介：魏郁林，男，1999年生，硕士生，济南大学材料科学与工程学院，山东 济南 250022，E-mail：wyldyx0712@163.com